THE ASTROPHYSICAL JOURNAL, 409:725–738, 1993 June 1


# CIRCUMSTELLAR SHELLS RESOLVED IN *IRAS* SURVEY DATA. II. ANALYSIS

K. YOUNG,[1] T. G. PHILLIPS,[1] AND G. R. KNAPP[2]
*Received 1992 February 19; accepted 1992 November 11*


## ABSTRACT

The *IRAS* survey data for 512 red giant stars and young planetary nebulae, most of which have been detected in rotational transitions of CO, were examined. The data for those objects which were not located in highly confused regions of the sky were processed using a computer program which fitted the data to an idealized model of a circumstellar shell. Of these stars 76 were found to have a circumstellar shell (CSS) that is resolved in the 60 $\mu$m survey data. Some of these stars are also resolved in the 100 $\mu$m survey data. Of the 76 stars, 40% are carbon stars. Three of the carbon stars, W Pic, RY Dra, and R CrB, have shells with radii of 3 pc or more. Only two of the resolved objects detectable in CO, NGC 2346 and IRC+10216, are surrounded by shells with masses $\gtrsim 1\ M_\odot$. Most of the nearby stars which are resolved are semiregular variables, while most of the nearby unresolved stars are Miras. No evidence was found that the shapes of the shells were distorted by interaction with the ISM. The average dust temperature in the outer region of the shells is $\sim 35$ K. Using this temperature and the mass-loss rates derived from observations of the inner shell, it is shown that the expansion velocity of the dust cannot greatly exceed that of the gaseous material. Some of the shells appear to be detached from the central star. The distribution of the inner radii of the detached shells indicates that CO is dissociated at a distance of $\sim 0.3$ pc from the star. Analysis of the colors of the shells resolved in both the 60 and 100 $\mu$m bands shows that the central star is the dominant dust heating source at radii less than $\sim 0.5$ pc, whereas an external source dominates beyond $\sim 1$ pc. Thirteen of the stars found to be extended are Mira variables. A simple model of the evolution of these shells, involving the interaction of the expelled material with the ISM, suggests that the period during which Mira variables lose mass lasts for $\sim 10^5$ yr. The same model indicates that carbon stars shed mass for $\sim 2 \times 10^5$ yr. For the largest shells the expansion velocity of the outer shell will typically be lower than the expansion velocity obtained from CO observations, by a factor of 3–5.


*Subject headings:* circumstellar matter — infrared: stars — planetary nebulae: general — stars: late-type — stars: mass-loss

## 1. INTRODUCTION

Much of the mass returned to the interstellar medium by stellar evolution processes is shed during the asymptotic giant branch (AGB) stage (Knapp & Morris 1985). AGB stars are cool ($T_{\rm eff} \leq 2000$ K), very luminous ($L_{\rm bol} \sim 10^4\ L_\odot$), and are observed to shed mass copiously, with observed mass-loss rates in the range $10^{-8}$ to $10^{-4}\ M_\odot\ {\rm yr}^{-1}$ (Knapp et al. 1982). Since the stars are cool, the mass is shed in the form of molecules and dust and can therefore be studied at radio, millimeter, and infrared wavelengths. Studies of the mass shed by evolved stars are important for understanding stellar evolution, for example, why so few stars ever approach the theoretical peak luminosity for an AGB star (Reid, Tinney, & Mould 1990) as well as the formation of planetary nebulae, the initial mass range of the progenitors of Type I supernovae, and the chemical evolution of our Galaxy's interstellar medium. The focus of the work presented here is on measuring the angular extent of the emission from circumstellar dust in these envelopes. Molecular line observations tell us the velocity at which material is expelled from the star, and, together with an estimate of the distance, the envelope extent yields the linear size and age of the envelope. Since the molecular line observations also give estimates of the stellar mass-loss rate, the total envelope mass can be found. We can then obtain a lower limit for the mass lost by these stars (which, given data on a large enough sample of objects, can be used to give an estimate of the total mass returned to the interstellar medium).

At first sight, it might be thought that these goals could be accomplished by mapping the millimeter wavelength molecular line emission, but the sizes of molecular envelopes are truncated by photodissociation (Letzelter et al. 1987; Mamon, Glassgold, & Huggins 1988). Also, although H I is not photodestroyed in the normal interstellar radiation field, the 21 cm emission from the circumstellar shells is extremely weak, and H I is ubiquitous and strong in the Galactic disk, so that H I observations are of very limited utility for this work (Knapp & Bowers 1988).

The *IRAS* Point Source Catalog (1985, hereafter PSC) contains some 246,000 detections, of which about 81,000 have colors suggesting the presence of circumstellar emission (Olofsson 1988; van der Vee & Habing 1988). We wished to determine which of these stars had a CSS which had been spatially resolved in the *IRAS* survey. An AGB star with a luminosity of $2 \times 10^4\ L_\odot$ and an effective temperature of 2000 K could be as distant as 2.5 kpc, and still have a 60 $\mu$m flux density above the PSC cutoff of 0.5 Jy. If that same star were obscured by a thick dust shell with a temperature of a few hundred K, it could be detected anywhere within our Galaxy. However, since a typical large CSS is expected to have a radius of about 0.3 pc (Rowan-Robinson et al. 1986), it must be no further than 1 kpc to be resolved by the 60″ beam *IRAS* provided at 60 $\mu$m. We therefore needed a way to select the small percentage of AGBs in the PSC which were nearby and had

[1] California Institute of Technology, Pasadena, CA 91125.
[2] Department of Astrophysical Sciences, Princeton University, Princeton, NJ 08544.

large circumstellar envelopes. Initially we chose to examine only those stars which have been detected in a rotational transition of CO. Such a star must be relatively nearby and have a large envelope, or else telescope beam dilution would prevent detection of its molecular line emission. In addition, the CO observations provide a direct measurement of the envelope's outflow velocity within the region $\lesssim 0.1$ pc from the star (Olofsson 1989), and an estimate of the star's mass-loss rate. We knew of at least one star, R CrB, which has a very large dust envelope (Gillet et al. 1986) but which has not been detected in CO, despite having been examined in several CO surveys (e.g., Wannier et al. 1990; Zuckerman & Dyck 1986a). In order to find other such shells, we looked at many additional stars selected by their *IRAS* colors and catalog associations. Stars from this second group will be referred to as the Additional List, and the prescription by which its members were selected is given in Young, Phillips, & Knapp (1992b, hereafter Paper I).

We found a total of 76 stars which appear to have CSS shell radii greater than 2′ in the *IRAS* 60 $\mu$m data. The details of how we examined the stars for signs of extended emission, as well tables and figures presenting the results, are also presented in Paper I.

## 2. PHYSICAL PARAMETERS

The angular size may be used to calculate the linear size of the CSS once the distance to the star is known. Table 1 lists the estimated distance and calculated envelope size for each star. The distance estimates were culled from the literature when available. Otherwise, the distances were estimated in one of the following ways. For the Mira variables, the period-luminosity-spectral type relationship (Bowers & Hagen 1984) was used to calculate $M_v$, then $m_v$ was used along with an estimate of the extinction, to calculate the distance. This technique was analyzed by Celis (1981), who estimated that the mean error in the derived distance is 19%. All other stars without published distances were assumed to have $M_K = -8.1$ (Kleinmann 1989). The $M_K$ was obtained from either the 2 $\mu$m sky survey (TMSS) or the survey of Fouqué et al. (1992), and extinction was ignored when the distance was calculated.

If it weren't for the interstellar medium, the age of each CSS could easily be calculated from its size and the expansion velocity obtained from CO observations. However the ISM should appreciably slow the expanding envelope once the density of the expanding shell has decreased to equal the density of the ISM. If the star's envelope is expanding at 15 km $s^{-1}$ and the mass-loss rate is $10^{-6}\ M_\odot\ yr^{-1}$, equal density will occur at a shell radius of 0.3 pc, assuming an ISM density of 1 H $cm^{-3}$. The envelope will have expanded to this size after only $2 \times 10^4$ yr, which is much shorter than the period of time that any star remains on the AGB. Therefore the effect of the ISM on the shell expansion cannot be ignored.

The mean free path for scattering against hydrogen atoms even at a low ISM density of 1 H $cm^{-3}$ is only $\sim 10^{-3}$ pc, so we can assume that the interaction between the ISM and the stellar wind occurs very near the edge of the expanding shell. The shell loses speed as it expands into the ISM and must accelerate the ambient material. Once the outer edge has been slowed by the ISM it will be pushed by material behind it which is still expanding at the original outflow speed.

The rate at which the outer edge expands can easily be calculated. Let $p$ be the total momentum of the expanding envelope edge, moving with a speed of $v$ and having mass $m$ (see Fig. 1):

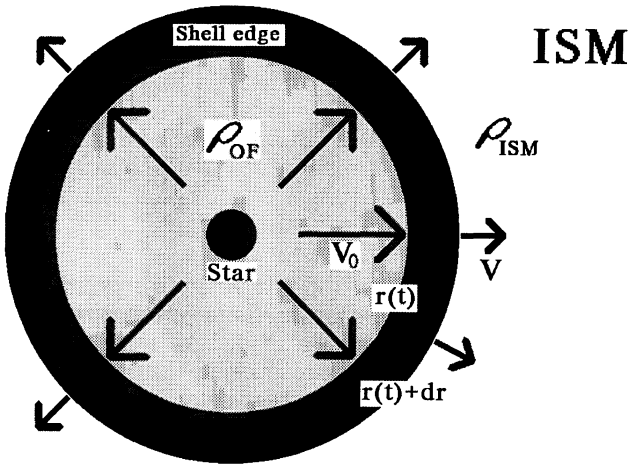


FIG. 1.—A dust shell expanding into the ISM. The leading edge of the expanding shell is slowed as it sweeps up material from the ISM. The edge is prevented from slowing to a halt by the pressure of the material behind it, which is still moving at the original speed of $v_0$.

$$F = \frac{dp}{dt} = v\frac{dm}{dt} + m\frac{dv}{dt}\,. \tag{1}$$

The material behind the shell edge is still moving with its original expansion velocity $v_0$, and it exerts a force on the shell edge of

$$F = 4\pi r^2 v_0\,\rho_{OF}(v_0 - v)\,,$$

where $r$ is the shell's outer radius. This force acts to maintain the velocity of the expanding shell. During a short time interval of length $dt$, the shell edge gains material of mass

$$dm = 4\pi r^2 \rho_{OF}(v_0 - v)dt + 4\pi r^2 \rho_{ISM}\, v\, dt\,. \tag{2}$$

The first term in $dm$ accounts for the stellar wind colliding with the edge from behind, and the second term accounts for the mass of ISM material that is swept up. If the mass-loss rate $\dot{M}$ and outflow speed $v_0$ are assumed to be constant, then

$$\rho_{OF} = \frac{\dot{M}}{4\pi r^2 v_0}\,. \tag{3}$$

With these assumptions equation (2) can be integrated to give the total mass of the shell edge

$$m = 4\pi \int_0^t r^2 \left[\rho_{OF}\left(v_0 - \frac{dr}{dt}\right) + \rho_{ISM}\frac{dr}{dt}\right]dt$$
$$= \dot{M}\left(t - \frac{r}{v_0}\right) + \frac{4}{3}\pi r^3 \rho_{ISM}\,. \tag{4}$$

Substituting equations (2) and (4) into equation (1) gives

$$4\pi r^2 v_0\,\rho_{OF}\left(v_0 - \frac{dr}{dt}\right) = 4\pi r^2\left[\rho_{OF}\left(v_0 - \frac{dr}{dt}\right) + \rho_{ISM}\frac{dr}{dt}\right]\frac{dr}{dt}$$
$$+ \left[\dot{M}\left(t - \frac{r}{v_0}\right) + \frac{4}{3}\pi r^3 \rho_{ISM}\right]\frac{d^2 r}{dt^2}\,.$$

The above equation can be solved for $d^2r/dt^2 = dv/dt$, yielding equations (5a) and (5b), a system of two coupled differential

TABLE 1

SHELL SIZES, AGES, AND MASSES

| (1) Name | (2) Distance (pc) | (3) Ref. | (4) Radius Outer | (5) Radius Inner | (6) $V_0$ (km s$^{-1}$) | (7) $10^7 \times \dot{M}$ ($M_\odot$ yr$^{-1}$) | (8) Ref. for (6) & (7) | (9) Age ($10^3$ yr) | (10) Mass ($M_\odot$) | (11) Spectral Type | (12) Class |
|---|---|---|---|---|---|---|---|---|---|---|---|
| AQ And | 870 | 17 | 0.84 | < 0.25 | ... | ... | ... | ... | ... | N | SR |
| R Scl | 400 | 1 | 0.76 | 0.13 | 24.7 | 71.0 | 3 D | 32 | 0.23 | C6II | SRb |
| CRL 278 | 250 | 9 | 0.37 | < 0.07 | 7.6 | 1.9 | 10 B | 73 | 0.014 | M7III | ... |
| o Cet A | 100 | 19 | 0.06 | < 0.03 | 5.0 | 11.0 | 3 D | 12 | 0.013 | M5e–M9e | Mira |
| UX And E | 420 | 9 | 0.44 | < 0.12 | ... | ... | ... | ... | ... | M6III | SRb |
| V Eri | 310 | 9 | 0.73 | 0.25 | 13.0 | 1.5 | 10 B | 96 | 0.014 | M5/M6IV | SRc |
| U Men E | 490 | 20 | 1.9 | 0.56 | ... | ... | ... | ... | ... | M3 | SR |
| R Dor | 60 | 21 | 0.12 | < 0.02 | ... | ... | ... | ... | ... | M8IIIq:e | SRb |
| ST Cam | 480 | 2 | 0.43 | < 0.14 | 10.0 | 1.6 | 2 | 67 | 0.011 | N5 | SRb |
| R Lep | 410 | 1 | 0.57 | < 0.12 | 20.5 | 17.0 | 3 D | 33 | 0.057 | C6IIe | Mira |
| W Ori | 340 | 2 | 0.63 | 0.21 | 11.8 | 1.9 | 2 | 96 | 0.018 | C5II | SRb |
| R Aur | 370 | 3 | 0.42 | < 0.11 | 10.9 | 5.3 | 3 D | 55 | 0.029 | M7IIIe | Mira |
| R Oct E | 500 | 22 | 1.5 | 0.77 | ... | ... | ... | ... | ... | M5.5e | Mira |
| W Pic | 660 | 1 | 1.2 | 0.19 | 7.0 | 0.5 | 1 | 310 | 0.016 | N | Lb |
| $\alpha$ Ori A | 200 | 3 | 0.61 | < 0.06 | 15.0 | 5.6 | 3 D | 75 | 0.042 | M2I | SRc |
| U Ori | 240 | 4 | 0.48 | 0.09 | 7.5 | 2.7 | 14 | 110 | 0.030 | M6.5IIIe | Mira |
| UU Aur | 290 | 2 | 0.36 | < 0.08 | 13.4 | 2.4 | 5 D | 43 | 0.010 | CII | SRb |
| IRC−10139 F | 570 | 9 | 2.7 | 0.46 | ... | ... | ... | ... | ... | M1Iab | ... |
| NGC 2346 | 460 | 5 | 0.84 | 0.20 | 19.0 | 100.0 | 5 | 57 | 0.57 | C envelope | PN |
| Y Lyn | 330 | 9 | 0.41 | 0.13 | 5.4 | 0.73 | 8 B | 120 | 0.008 | M5Ib-II | SRc |
| KK Car E | 470 | 9 | 1.5 | 0.44 | ... | ... | ... | ... | ... | M3pe | Mira |
| X Cnc | 460 | 2 | 1.2 | 0.16 | 12.0 | 2.7 | 2 | 170 | 0.045 | CII | SRb |
| RS Cnc | 200 | 9 | 0.33 | 0.06 | 5.3 | 0.69 | 3 D | 90 | 0.006 | M6IIIase | SRc? |
| R Leo | 120 | 24 | 0.13 | < 0.03 | 4.0 | 0.14 | 3 D | 47 | 0.001 | M8IIIe | Mira |
| Y Hya | 510 | 1 | 1.4 | 0.19 | 10.2 | 2.0 | 1 | 290 | 0.058 | C | SRb |
| CIT 6 A | 190 | 3 | 0.39 | < 0.06 | 16.9 | 30.0 | 3 D | 26 | 0.077 | C envelope | Mira |
| U Ant | 320 | 1 | 0.43 | < 0.09 | 21.2 | 14.0 | 1 | 27 | 0.038 | N | Lb |
| U Hya | 290 | 1 | 0.24 | 0.11 | 7.9 | 1.2 | 1 | 37 | 0.004 | CII | SRb |
| VY UMa | 520 | 2 | 0.46 | < 0.15 | 8.4 | 1.3 | 2 | 64 | 0.008 | C5II | Lb |
| R Crt | 240 | 9 | 0.41 | 0.13 | 11.0 | 2.3 | 10 B | 88 | 0.002 | M7III | SRb |
| IRC−30163E | 300 | 13 | 0.59 | 0.20 | 8.0 | 1.2 | 10 B | 140 | 0.017 | M7III | ... |
| RU Crt | 450 | 9 | 0.38 | < 0.13 | ... | ... | ... | ... | ... | M3 | Lb? |
| BK Vir | 280 | 9 | 0.45 | 0.12 | 4.7 | 0.48 | 11 B | 130 | 0.006 | M7III | SRb |
| Y UMa | 330 | 9 | 0.36 | 0.16 | 4.7 | 0.67 | 11 B | 92 | 0.006 | M7II-III | SRb |
| Y CVn | 280 | 2 | 0.45 | 0.23 | 9.0 | 1.1 | 2 | 66 | 0.007 | CIab | SRb |
| RY Dra | 450 | 2 | 2.5 | 0.25 | 10.0 | 1.8 | 2 | 500 | 0.090 | C | SRb |
| RT Vir | 270 | 3 | 0.32 | 0.08 | 11.3 | 2.2 | 3 D | 34 | 0.007 | M8III | SRb |
| SW Vir | 210 | 13 | 0.70 | < 0.06 | 9.4 | 3.2 | 6 | 110 | 0.035 | M7III | SRb |
| R Hya | 110 | 19 | 0.18 | 0.06 | 7.5 | 0.22 | 8 B | 42 | 0.001 | M7IIIe | Mira |
| W Hya | 80 | 19 | 0.24 | < 0.02 | 9.7 | 0.20 | 8 B | 58 | 0.001 | M8e | SRa |
| $\theta$ Aps E | 320 | 21 | 1.1 | < 0.09 | ... | ... | ... | ... | ... | M6.5III | SRb |
| RX Boo | 140 | 19 | 0.27 | < 0.04 | 11.5 | 1.5 | 3 D | 32 | 0.005 | M7.5e | SRb |
| RW Boo E | 490 | 9 | 0.71 | 0.20 | ... | ... | ... | ... | ... | M5III | SRb |
| X TrA | 300 | 1 | 0.36 | 0.11 | 9.2 | 0.9 | 1 | 73 | 0.007 | C5 | Lb |
| R CrB G | 1600 | 23 | 4.6 | 0.70 | ... | ... | ... | ... | ... | G0Iab:pe | R CrB |
| ST Her | 290 | 9 | 0.48 | < 0.08 | 6.0 | 0.33 | 26 B | 130 | 0.004 | M6s | SRb |
| X Her | 220 | 9 | 0.39 | < 0.06 | 8.5 | 1.4 | 8 B | 65 | 0.009 | M8e | SRb |
| S Dra | 430 | 9 | 0.96 | 0.25 | 8.3 | 0.61 | 27 B | 220 | 0.013 | M6III | SRb |
| V Pav | 460 | 9 | 0.51 | 0.17 | 16.0 | 3.1 | 27 B | 52 | 0.016 | C+ | SRa |
| NGC 6720 C | 780 | 15 | 1.2 | < 0.23 | 24.0 | ... | 16 | ... | ... | ... | PN |
| $\delta^2$ Lyr | 360 | 21 | 1.7 | 0.41 | ... | ... | ... | ... | ... | M4II | SRc? |
| V Tel E | 430 | 9 | 0.68 | 0.21 | ... | ... | ... | ... | ... | M7 | SRb |
| V1942 Sgr | 630 | 1 | 0.59 | < 0.18 | 10.0 | 1.1 | 1 | 110 | 0.012 | CII | Lb |
| UX Dra | 430 | 2 | 0.50 | < 0.13 | 6.9 | 1.8 | 2 | 100 | 0.018 | CII | SRa |

TABLE 1—*Continued*

| (1) Name | (2) (3) Distance (pc) | Ref. | (4) (5) Radius Outer | Inner | (6) $V_0$ (km s$^{-1}$) | (7) $10^7 \times \dot{M}$ ($M_\odot$ yr$^{-1}$) | (8) Ref. for (6) & (7) | (9) Age ($10^3$ yr) | (10) Mass ($M_\odot$) | (11) Spectral Type | (12) Class |
|---|---|---|---|---|---|---|---|---|---|---|---|
| AQ Sgr | 570 | 1 | 0.50 | 0.20 | 6.0 | 1.8 | 6 | 120 | 0.021 | CII | SRb |
| R Cyg [A] | 420 | 5 | 0.59 | 0.24 | 11.3 | 1.6 | 5 | 100 | 0.016 | S | Mira |
| S Pav [E] | 210 | 19 | 0.42 | < 0.06 | ... | ... | ... | ... | ... | M7IIe | SRc |
| V1943 Sgr | 300 | 7 | 0.43 | < 0.09 | 8.0 | 1.9 | 6 | 76 | 0.015 | M7III | Lb |
| X Pav | 240 | 9 | 0.35 | < 0.07 | 10.5 | 1.9 | 18 [B] | 37 | 0.009 | Mc | SRa |
| RZ Sgr | 660 | 9 | 0.82 | 0.19 | 12.5 | 15.0 | 27 [B] | 72 | 0.11 | Se | SRb |
| RT Cap | 510 | 1 | 1.2 | 0.15 | 9.1 | 0.6 | 1 | 320 | 0.019 | CII | SRb |
| T Mic | 200 | 9 | 0.33 | < 0.06 | 8.1 | 0.27 | 27 [B] | 83 | 0.002 | M7III | SRb |
| T Ind | 550 | 1 | 0.46 | < 0.16 | 5.5 | 0.4 | 1 | 100 | 0.004 | CII | SRb |
| Y Pav | 450 | 1 | 0.75 | < 0.13 | 9.4 | 1.5 | 1 | 120 | 0.017 | CII | SRb |
| S Cep | 300 | 4 | 0.33 | < 0.09 | 22.4 | 5.3 | 10 [B] | 20 | 0.011 | CII | Mira |
| RV Cyg | 470 | 2 | 0.82 | 0.21 | 14.7 | 5.6 | 2 | 100 | 0.057 | CII | SRb |
| EP Aqr | 200 | 9 | 0.35 | 0.09 | 8.6 | 2.0 | 10 [B] | 56 | 0.011 | M8III | SRb |
| PQ Cep | 710 | 13 | 1.5 | 0.43 | 21.7 | 17.0 | 12 [B] | 110 | 0.19 | C | ... |
| W Peg | 270 | 19 | 0.57 | 0.27 | 6.4 | 0.68 | 14 | 160 | 0.011 | M7e | Mira |
| SV Peg | 320 | 9 | 0.44 | 0.14 | 11.0 | 0.76 | 25 [B] | 82 | 0.006 | M | SRa |
| $\pi^1$ Gru | 200 | 7 | 0.28 | < 0.06 | 14.9 | 13.0 | 6 | 21 | 0.027 | S5 | SRb |
| V PsA | 330 | 7 | 0.49 | 0.12 | 21.0 | 6.9 | 6 | 27 | 0.019 | M7III | SRb |
| TX Psc | 280 | 1 | 0.25 | < 0.08 | 12.1 | 0.7 | 1 [B] | 27 | 0.002 | CII | Lb |
| RS And [E] | 440 | 9 | 2.5 | 0.45 | ... | ... | ... | ... | ... | M7–M10 | SRa |
| R Cas | 220 | 3 | 0.27 | 0.06 | 12.3 | 5.1 | 3 | 29 | 0.015 | M7IIIe | Mira |

[a] These results are from processing the small data set provided by the default ADDSCAN parameters. All others used the data set obtained by changing the ADDSCAN search radius to 10′.

[b] The mass-loss rates for these objects were calculated from the CO (1–0) or CO (2–1) line strengths and widths, using formula (9a) or (9b) from van der Veen & Rugers 1989.

[c] Much of the molecular envelope of NGC 6720 has been dissociated by the central star, therefore observations of CO cannot be used to determine the precursor star's mass-loss rate.

[d] The value for $\dot{M}$ has been rescaled for our estimate of the distance.

[e] Observed, but not detected in a CO (1–0) survey by Nyman et al. 1992.

[f] Observed, but not detected in a CO (1–0) survey by Heske 1989.

[g] Observed, but not detected in a CO (2–1) survey by Wannier et al. 1990.

REFERENCES.—(1) Olofsson et al. 1988; (2) Olofsson et al. 1987; (3) Knapp & Morris 1985; (4) Using P-L-S, relationship from Bowers & Hagen 1984; (5) Knapp 1986; (6) Knapp unpublished; (7) Knapp et al. 1992; (8) Wannier & Sahai 1986; (9) Using the *K*-magnitude from the IRC or Fouqué et al. 1992, and assuming an absolute *K*-magnitude of −8.1 (Kleinmann 1989); (10) Zuckerman & Dyck 1986a; (11) Zuckerman & Dyck 1989; (12) Zuckerman et al. 1986; (13) van der Veen & Rugers 1989; (14) An unpublished CO (3–2) spectrum taken at the CSO was used, along with an LVG radiative transfer program (Morris 1980); (15) Huggins & Healey 1986; (16) Leene & Pottasch 1988; (17) Claussen et al. 1987; (18) Deguchi et al. 1990; (19) Jura & Kleinmann 1992; (20) van den Bergh 1984; (21) Judge & Stencel 1991; (22) Onaka et al. 1989; (23) Gillet et al. 1986; (24) Gatewood 1992; (25) Zuckerman & Dyck 1986b; (26) Margulis et al. 1990; (27) Nyman et al. 1992.

equations which can be solved to give the shell's radius as a function of time:

$$\frac{dr}{dt} = v\,, \tag{5a}$$

$$\frac{dv}{dt} = \frac{\dot{M}(v_0 - v) - [\dot{M}(1 - v/v_0) + 4\pi r^2 v \rho_{\rm ISM}]v}{\dot{M}(t - r/v_0) + \frac{4}{3}\pi r^3 \rho_{\rm ISM}}\,. \tag{5b}$$

Equations (5a) and (5b) were numerically integrated to solve for the age of each CO-detected star which was found to be extended. For consistency, the CSS radius from the 60 $\mu$m data was used in all cases, even if a 100 $\mu$m radius was available. The results are given in Table 1. The ISM density was assumed to fall off exponentially, in the direction $z$ perpendicular to the Galactic plane, from a value of 2 H cm$^{-3}$ (Spitzer 1978), with a scale height of 100 pc (Mihalas & Binney 1981). As is shown by Figure 2, the expansion rate of the shell edge is not strongly dependent upon $\rho_{\rm ISM}$; the final size of the shell is reduced by less than a factor of 2 when $\rho_{\rm ISM}$ is increased by a factor of 10. The mass-loss rates were taken from calculations in the literature. These calculations were made by solving the radiative transfer problem for thermal CO emission using the Sobolev approximation (Knapp & Morris 1985), and they are not dependent on any measurements of the continuum emission from the CSS. If our assumed distance differed from the value that had been used to calculate $\dot{M}$, we rescaled the value assuming that $\dot{M} \propto D^2$, which is appropriate if, as was usually the case, the molecular envelope was unresolved. The dust was assumed to have been ejected from the star at the terminal velocity derived from the CO profile. The velocity difference between the dust and the gas (the "drift velocity") was ignored, which is apt to have caused us to overestimate the shell's age. While the drift velocity is probably small for optically thick shells with $\dot{M} \geq 2 \times 10^{-5}\ M_\odot\ {\rm yr}^{-1}$ (Gail & Sedlmayr 1985), calculations for the drift velocity in optically thin shells (Berruyer & Frisch 1983; Goldreich & Scoville 1976) predict drift velocities larger than the terminal velocity for the molecular material. Dougados, Rouan, & Léna (1992) directly determined the dust velocity of the inner ~0.01 pc of IRAS 09371+1212, by measuring Doppler shifts in the scattered photospheric emission. They found dust velocities 10–15 km s$^{-1}$ *lower* than the CO velocity (i.e., a negative drift velocity).

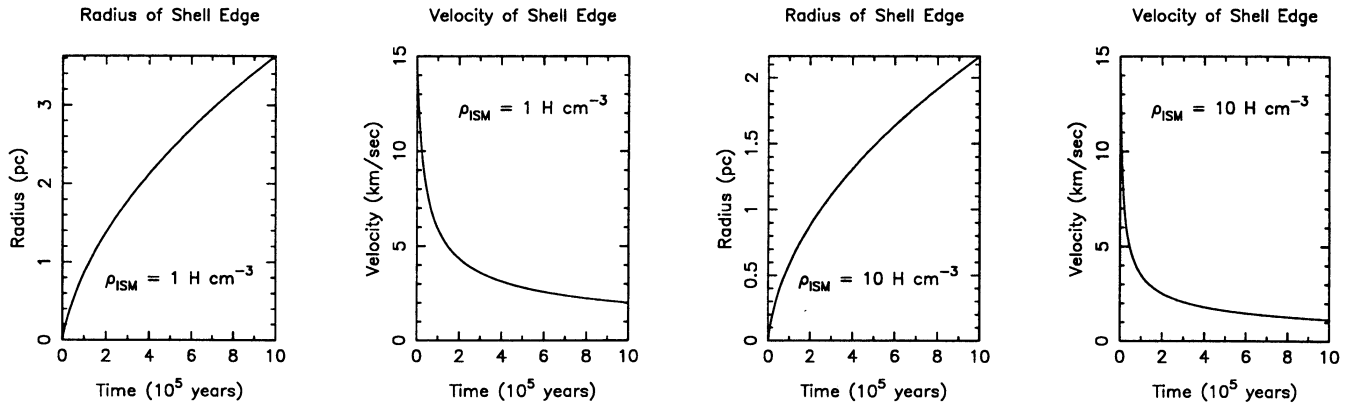


FIG. 2.—Results of numerically integrating eqs. (5a) and (5b) are shown for two values of the ISM density $\rho_{ISM}$. In both cases $\dot{M} = 10^{-6}\ M_\odot\ \mathrm{yr}^{-1}$ and $v_0 = 15$ km s$^{-1}$. The period of copious mass-loss for an AGB star probably lasts for $\sim 5 \times 10^5$ yr, and over that period the expansion velocity of the shell edge drops from 15 to under 3 km s$^{-1}$. This deceleration would be difficult to detect from molecular line observations. The CO envelope is expected to be truncated at a radius of about 0.3 pc by photodissociation, even for very large mass-loss rates (Mamon et al. 1988). If the CSS has expanded beyond the dissociation radius, then the molecular emission lines won't show signs of deceleration because the molecular material will only be present in a region where the ISM has already been swept away. On the other hand, if the CSS has not yet expanded to the dissociation radius, the shell is so small that the velocity of the shell edge will not yet have been significantly reduced.

While these authors show that the apparent dust velocity could be lowered by a variety of radiative transfer effects, their data certainly do not support large drift velocities. In the outer regions of the envelope it is unlikely that the drift velocity can greatly exceed 20 km s$^{-1}$, because beyond that velocity the grains will be destroyed by sputtering (Kwok 1975). The fact that extended continuum emission surrounding these stars is visible at all places an upper limit on the magnitude of the drift velocity (see § 2.4).

The value for the total shell mass in column (10) of Table 1 is the product of the estimated age multiplied by the mass-loss rate from CO observations. Calculating the mass in this way assumes that $\dot{M}$ is constant over periods comparable with its AGB lifetime, which is almost certainly not true. Evidence suggests that the mass-loss rate increases as the star progresses up the AGB (Iben & Renzini 1983), so our use of the CO-derived mass-loss rate (which samples only material ejected within the last few thousand years) is apt to result in the total mass being overestimated. With the exception of NGC 2346, the estimated masses are strikingly small when one considers that an average star is expected to shed $\sim 1\ M_\odot$ during its AGB lifetime (Herman & Habing 1985). IRC+10216 was not included in Table 1, because its 60 $\mu$m *IRAS* data is so anomalous. If we combine IRC+10216's 100 $\mu$m size with the distance, expansion velocity and mass-loss rate from Knapp & Morris (1985), we obtain a CSS with a radius of 0.8 pc containing 3 $M_\odot$ of material. It appears that only IRC+10216, out of all the red giants in the solar neighborhood, and the planetary nebula NGC 2346 have lost a significant fraction of their total envelope mass. This strongly implies that mass is not lost at a constant rate on the AGB, or even at a gradually increasing rate, but rather most of an AGB star's envelope is ejected during a brief period which may terminate the AGB phase.

The average radius of the shells in Table 1 is 0.74 pc. Since this table consists only of those stars which appear to have been resolved, stars with large shells are overrepresented. The shells surrounding 28 of the stars are at least twice as large as the maximum size of 0.3 pc predicted by Rowan-Robinson et al. (1986). The mass-loss rates and ages from Table 1 show no correlation.

### 2.1. *Detached Shells*

One of the parameters fitted by our model fitting program (MFP) was the inner radius of the CSS. Table 3 of Paper I lists these radii in angular units, while the value in pc is given here in Table 1 (if the radius is less than the 1′ resolution of *IRAS* at 60 $\mu$m, an upper limit corresponding to 1′ is given). Nineteen of the stars have radii larger than 1.′5. These stars may have entered a quiescent period of reduced mass loss. Figure 3 shows the 60 and 100 $\mu$m maps produced by analyzing the survey data for Y CVn with the IPAC HIRES processor (Aumann, Fowler, & Melnyk 1990). While the HIRES image shows that the CSS has a more complex structure than the simple dust model used by the MFP, the outer edge of the MFP model dust shell matches the maximum extent of emission in the map quite well. The MFP calculated an inner radius of 2.′8 for the 60 $\mu$m data, and the map also shows a similar inner radius for the extended emission. However the 1.′2 inner radius derived from the 100 $\mu$m data is nearly equal to the resolution of *IRAS* at 100 $\mu$m and probably has no physical significance.

If the inner radii reported by the MFP are not spurious, then one would expect those shells with large inner radii to lack the spectral features associated with high-density gas. Maser emission from OH, $H_2O$, and SiO arise from radii of about $10^{16}$, $10^{15}$, and $10^{13}$ cm, respectively (Herman & Habing 1985). SiO thermal emission also traces higher density material than CO, because of its much larger dipole moment. Table 2 lists which of the oxygen-rich objects with inner radii larger than the *IRAS* diffraction limit have emission from these high-density tracers. All but two of the seven objects with inner radii less than 0.1 pc show one of these lines, while only six of the 20 objects with a larger inner radius do. For the shells with inner radii larger than 0.3 pc, even the thermal CO emission is absent. These trends indicate that the inner radii fitted by the MFP are physically significant.

Figure 4*a* shows a histogram of the CSS inner radii. While the largest number of shells have very small inner radii, those stars whose inner radii were actually resolved have a fairly uniform distribution between 0.05 and 0.25 pc. The distribu-

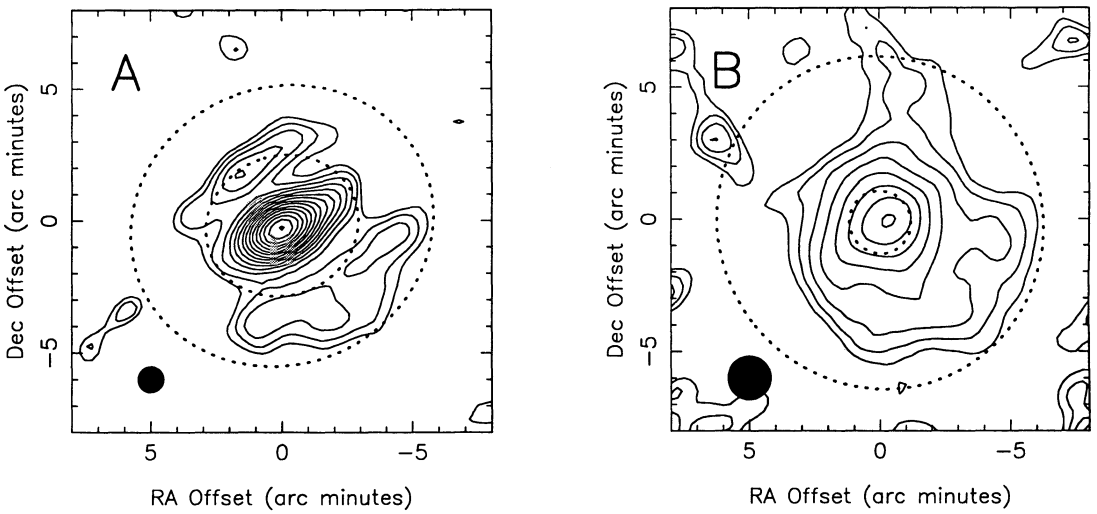


FIG. 3.—Results of processing the survey data covering Y CVn with the IPAC HIRES program suite are shown. In (*a*), the 60 $\mu$m map, the lowest contour level is 0.45% of the peak intensity, and the contours are logarithmically spaced with ratios of 1.5. The central source appears elongated, however, this is almost certainly an artifact caused by the large size of the 60 $\mu$m detectors in the cross-scan direction. Panel (*b*) shows the 100 $\mu$m HIRES map. Here the lowest contour is 2% of peak intensity, and the ratio between successive contours is 1.7. In both panels the inner and outer extents of the dust model fitted by the MFP are shown as dotted lines. The filled circles show the *IRAS* resolution (80% encircled energy).

tion falls off dramatically beyond 0.3 pc, and all but one of the seven objects with inner radii larger than 0.3 pc do not have a detectable CO envelope. This suggests that the CO is photodissociated at a radius of 0.25–0.30 pc. This is in good agreement with the CO radius calculated by Mamon et al. (1988) for stars with very large mass-loss rates ($\dot{M} > 10^{-5}\ M_{\odot}\ \mathrm{yr}^{-1}$).

Figure 4*b* shows the age of 59 of the dust shells from Table 1, plotted as a function of the inner shell radius in parsecs. These two quantities appear to be weakly correlated. The linear correlation constant, $r$, for these two variables is 0.48. The probability of $r$ having this high a value if the age and inner shell radius are uncorrelated is less than 0.001 (Young 1962). However, since the age of the shell is strongly correlated with its *outer* radius ($r = 0.85$), a spurious correlation could occur between the age and the inner radius. This would happen if the assumed dust emission profile or the MFP itself had a defect which caused shells with large outer radii to be fitted with large inner radii. Since the outer radii must be larger than the inner radii, the two radii will be correlated even if the MFP is not defective, and this tautologous correlation could give rise to an age—inner radius correlation. There is no correlation between the *IRAS* colors of the object, and the shell's inner radius. This is surprising if the calculated inner radii are correct, since one would expect a detached shell to be cooler, allowing the star's photosphere to dominate the 12 and 25 $\mu$m bands.

If the weak correlation of age with inner radius is not spurious it suggests that the mass-loss process becomes more episodic as the star loses its atmosphere. For AGB stars, this might occur as a consequence of the thermal pulse cycle. Throughout the thermal pulse phase, the amplitude of the luminosity variation caused by a thermal pulse increases with each successive pulse (Iben & Renzini 1983). Since it is likely that the stellar winds from these stars are driven by radiation pressure, these luminosity variations could modulate the mass-loss rate and produce shells which appear to be detached from the central star.

TABLE 2

CO, OH, $H_2O$ AND SiO EMISSION FROM OXYGEN-RICH SHELLS WITH RESOLVED INNER RADII

| Name | $R_{inner}$ (pc) | CO | OH 1612 | $H_2O$ | SiO | Name | $R_{inner}$ (pc) | CO | OH 1612 | $H_2O$ | SiO |
|---|---|---|---|---|---|---|---|---|---|---|---|
| RS Cnc | 0.06 | T | ... | ... | ... | IRC−30163E | 0.20 | T | ... | (1) | ... |
| R Hya | 0.06 | T | ... | M | T | RW Boo | 0.20 | ... | ... | ... | ... |
| R Cas | 0.06 | T | ... | M | M | V Tel | 0.21 | ... | ... | (1) | ... |
| RT Vir | 0.08 | T | ... | M | T | R Cyg | 0.24 | T | ... | ... | ... |
| U Ori | 0.09 | T | M | M | T | V Eri | 0.25 | T | ... | ... | ... |
| EP Aqr | 0.09 | T | ... | ... | ... | S Dra | 0.25 | T | ... | ... | ... |
| V PsA | 0.12 | T | ... | ... | ... | W Peg | 0.27 | T | ... | M | T |
| BK Vir | 0.12 | T | ... | ... | ... | $\delta^2$ Lyr | 0.41 | (2) | ... | ... | ... |
| Y Lyn | 0.13 | T | ... | ... | ... | KK Car | 0.44 | ... | ... | (1) | ... |
| R Crt | 0.13 | T | ... | M | T | RS And | 0.45 | ... | ... | M | ... |
| SV Peg | 0.14 | T | ... | M | ... | IRC−10139 | 0.46 | ... | ... | ... | ... |
| Y UMa | 0.16 | T | ... | ... | ... | U Men | 0.56 | ... | ... | (1) | T |
| RZ Sgr | 0.19 | T | ... | (1) | ... | R Oct | 0.77 | ... | ... | (1) | T |

NOTES.—M = Maser emission, T = Thermal emission. (1) Not in the region covered by the catalog of $H_2O$ masers. (2) We were unable to locate any published detections or nondetections of rotational CO emission from this object. Sources: CO—see Table 1; OH 1612 masers—Hekkert et al. 1989; $H_2O$ masers—Cesaroni et al. 1988; SiO emission (thermal and maser)—Engels & Heske 1989.

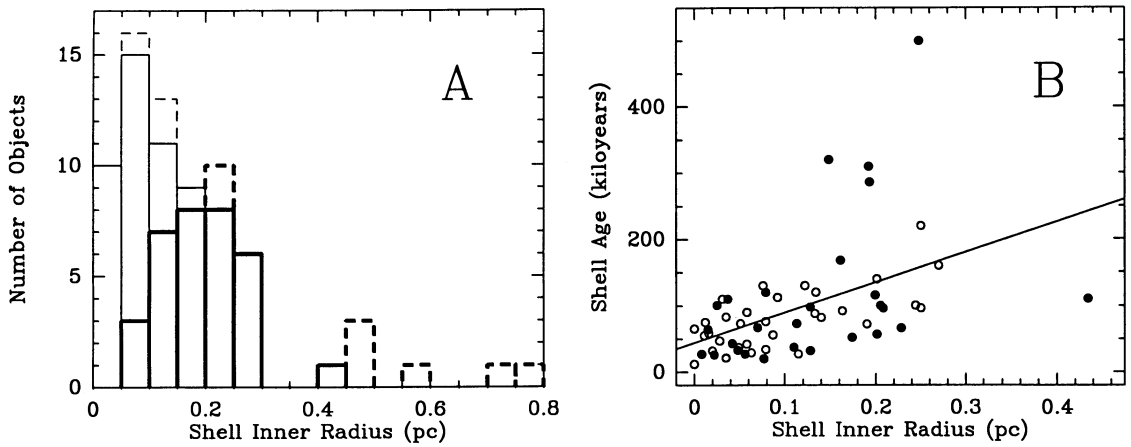


FIG. 4.—(*a*) A histogram of the inner shell radii is shown. The bold line histogram shows the values for those shells whose inner radii had an angular size of 1′ or more, and may have actually been resolved. The thin line histogram shows the values for objects whose fitted inner radii are smaller than the *IRAS* 60 μm diffraction limit, and probably have little or no physical significance. Solid lines are used for the objects which have been detected in CO, while a dashed line is used for objects with published nondetections. For the stars with CO emission, the radii are distributed rather uniformly through the range of 0.05–0.25 pc and only PQ Cep has an inner radius larger than 0.3 pc. (*b*) The calculated age of the dust shells for 59 of the stars in Table 1, plotted as a function of the inner shell radius. Carbon stars are plotted as filled circles; oxygen-rich objects are unfilled. NGC 6720 and the stars without CO detections were not included in this plot because their ages were not calculated. Also shown is the least-squares best-fit line. The weak correlation is stronger for the carbon-rich envelopes.

### 2.2. *Comparison of Resolved and Unresolved Objects*

For the remainder of this paper, unless stated otherwise, we will consider only those stars which have been detected in CO, because they form a more homogeneous group than do the stars from the Additional List. A large fraction of the stars with distances of 500 pc or less appear to be resolved (see Paper I). While seven of the eight stars with distances less than 200 pc are resolved in the 60 μm data, there are many stars within 500 pc which are not. The 33 unresolved stars which are within 500 pc are listed in Table 3. If we adopt Kleinmann's (1989) scale heights of 200 pc for carbon stars and 400 pc for oxygen-rich stars, the total number of stars in our CO-selected list (both resolved and unresolved) as a function of distance is well fitted by an exponential disk, out to a distance of 400 pc for the oxygen-rich stars, and 600 pc for the carbon stars. The best-fit space densities are 110 $kpc^{-3}$ for carbon stars and 270 $kpc^{-3}$ for oxygen-rich stars in the Galactic midplane (here and elsewhere in this paper N stars are grouped with carbon stars and S stars are considered oxygen-rich). Beyond 400 pc our list must be quite incomplete because the number of stars per unit distance drops off rapidly. The fact that the list of resolved stars in Table 1 contains nearly equal numbers of carbon and oxygen-rich objects, even though the oxygen-rich stars are twice as common, is a reflection of the larger average size of the carbon star shells.

The average distance to the unresolved stars is 370 pc. At that distance a CSS with a radius $\geq 0.2$ pc could be clearly resolved. This is less than one-third the average CSS size of the

TABLE 3

STARS WITHIN 500 pc WHICH ARE UNRESOLVED

| NAME | DISTANCE (pc) | Reference | $V_0$ (km $s^{-1}$) | Reference | CLASS | NAME | DISTANCE (pc) | Reference | $V_0$ (km $s^{-1}$) | Reference | CLASS |
|---|---|---|---|---|---|---|---|---|---|---|---|
| T Cas | 360 | 1 | 5.2 | 12 | Mira | RV Boo | 380 | 10 | 8.1 | 13 | SRb |
| R And | 310 | 2 | 8.7 | 2 | Mira | CRL 4211[a] | 330 | 4 | 20.5 | 4 | ... |
| UY Cet | 470 | 10 | 8.1 | 13 | SRb | S CrB | 300 | 8 | 7.8 | 17 | Mira |
| W And | 280 | 3 | 11.0 | 14 | Mira | IRAS 15194−5115[a] | 400 | 4 | 23.3 | 4 | ... |
| R Hor | 270 | 4 | 6.6 | 4 | Mira | R Ser | 330 | 8 | 5.6 | 17 | Mira |
| TW Hor[a] | 420 | 5 | 5.3 | 5 | SRb | RU Her | 370 | 1 | 9.2 | 17 | Mira |
| NML Tau | 270 | 2 | 22.0 | 2 | Mira | U Her | 360 | 3 | 11.6 | 17 | Mira |
| TX Cam | 360 | 2 | 16.9 | 15 | Mira | g Her | 160 | 9 | 10.0 | 15 | SRb |
| S Pic | 390 | 6 | 11.8 | 13 | Mira | IRC+10365 | 500 | 2 | 16.7 | 2 | ... |
| Y Tau[a] | 480 | 5 | 10.7 | 5 | SRa | X Oph | 300 | 1 | 5.5 | 17 | Mira |
| V Cam | 390 | 6 | 12.2 | 16 | Mira | RS CrA | 280 | 7 | 20.7 | 19 | ... |
| S CMi | 480 | 1 | 4.1 | 17 | Mira | W Aql | 470 | 2 | 19.9 | 2 | Mira |
| R Cnc | 310 | 1 | 3.4 | 17 | Mira | IRC+80040 | 500 | 10 | 12.0 | 20 | SRb |
| CRL 5254[a] | 420 | 7 | 12.8 | 12 | ... | T Cep | 200 | 1 | 5.0 | 16 | Mira |
| R LMi | 260 | 8 | 6.0 | 18 | Mira | V460 Cyg[a] | 440 | 11 | 11.4 | 11 | Lb |
| V Hya[a] | 400 | 2 | 20.9 | 2 | SRa | CRL 3099[a] | 500 | 2 | 10.1 | 2 | ... |
| S Vir | 450 | 8 | 3.5 | 17 | Mira | | | | | | |

[a] These stars are carbon stars or have carbon-rich envelopes.

SOURCES.—(1) Sivagnanam et al. 1988; (2) Knapp & Morris 1985; (3) Using P-L-S relationship from Bowers & Hagen 1984; (4) Knapp et al. 1989; (5) Olofsson et al. 1988; (6) Onaka et al. 1989; (7) van der Veen & Rugers 1989; (8) Jura & Kleinmann 1992; (9) Eaton & Johnson 1988; (10) Assuming an absolute *K*-magnitude of −8.1; (11) Olofsson et al. 1987; (12) Zuckerman & Dyck 1986a; (13) Lyman et al. 1992; (14) Zuckerman et al. 1986; (15) Wannier & Sahai 1986; (16) Zuckerman & Dyck 1989; (17) Young et al. 1992; (18) Knapp et al. 1982; (19) Zuckerman & Dyck 1986b; (20) Knapp (unpublished); (21) Zuckerman & Dyck 1989.

resolved stars listed in Table 1. Therefore if the distance estimates for the unresolved stars are not too low by a factor of 3 or more, their shells must either be much smaller on average than those of the resolved stars, or not dense enough to be detected by *IRAS*. If the unresolved stars have shells which are just as large as those of the resolved stars, but less dense, then either the mass-loss rates for these stars must be lower, or the outflow velocity must be higher. However, the average CO velocity for both the unresolved and resolved groups (excluding the resolved stars with distances greater than 500 pc, we shall call this group "the nearby resolved group") is 11 km $s^{-1}$. Radiative transfer models of the CO emission from evolved stars show that the mass-loss rate is strongly correlated with the expansion velocity (Knapp et al. 1982), so it is likely that the mass-loss rates of these two groups are also similar. Therefore the unresolved stars on average should not have less dense envelopes, implying that they must have smaller envelopes than those surrounding the resolved stars. Note, however, that the closest unresolved Miras do have very low expansion velocities and may have large undetectable shells (see below).

The envelopes surrounding the unresolved objects might be smaller for one of three reasons. The first possible reason is that the ISM surrounding the unresolved objects might be so dense that it confines the ejected material within a relatively small distance from the star. If the unresolved objects are in regions of very high ISM density, then they should cluster more closely about the Galactic plane, but they do not; the average absolute Galactic latitude of the unresolved objects is 29°2, which is not significantly different than the nearby resolved group's average value of 35°1 and merely reflects the larger average distance of the unresolved objects. The second possible reason is that the CSSs surrounding the unresolved objects have been stripped off by ram pressure arising from the star's large peculiar velocity. All but three of the resolved stars and two-thirds of the unresolved stars within 500 pc are near enough to have measurable proper motions. The proper motion may be combined with the radial velocity from the CO detections to calculate the full three-dimensional velocity of the star, with respect to the local standard of rest ($v_{LSR}$). For stars this near the Sun, $|v_{LSR}|$ should be a good approximation to the speed of the star with respect to its local interstellar medium. For the unresolved stars the average speed is $\overline{|v_{LSR}|} = 61.5$ km $s^{-1}$, which is slightly larger than the value of 54.8 km $s^{-1}$ obtained for the resolved stars. Also the average magnitude of the radial $v_{LSR}$, which is available from the CO observations for all the stars, is 18.1 km $s^{-1}$ for the unresolved stars and 15.5 km $s^{-1}$ for those which were resolved. While the unresolved stars do appear to be moving ~15% faster than the resolved ones, this difference is much less than the standard deviation of the velocities in either sample, and probably is just another reflection of the greater average distance to the unresolved stars. Therefore it does not seem likely that all the unresolved stars have had their envelopes stripped away by ram pressure. The third explanation for the unresolved stars is the simplest—perhaps they simply have not yet grown large enough to be resolved. If this is the case, the close agreement of the average CO expansion velocities in both groups tells us that the unresolved stars must be younger than the resolved ones.

A color-color diagram for these nearby unresolved stars, along with all the stars found to be resolved, is shown in Figure 5. While the stars found to be resolved are divided nearly evenly between carbon stars (27 objects) and oxygen-rich (M) stars (31 objects), only 8 of the 33 unresolved nearby stars are carbon stars. This suggests that the carbon stars have been losing mass for a longer time, on average, than have the M stars. The calculated shell ages in Table 1 provide additional evidence of this. The average age of the carbon star shells is $1.1 \times 10^5$ yr, whereas the average age of the oxygen-rich shells is $7.9 \times 10^4$ yr.

The Mira variables in Tables 1 and 3 are of particular interest. Since Miras obey a period-luminosity relationship, their distances can be estimated much more accurately than is possible for the other objects in this study. The average age of the shells around the resolved Miras in Table 1 is $5.7 \times 10^4$ yr.

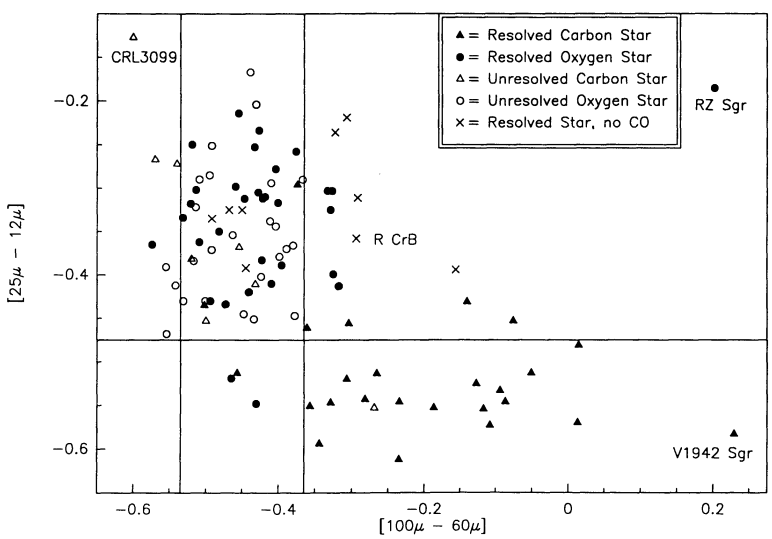


FIG. 5.—An *IRAS* two-color diagram is shown for all extended objects (*filled symbols*), including those beyond 500 pc, along with objects within 500 pc which were not found by the MFP to be extended (*open symbols*). No color corrections have been applied to the fluxes from the PSC. Not shown are two planetary nebulae with very blue [25 − 12] colors, NGC 6720 and NGC 2346. IRAS 09372+1212, Y Hya, and IRC −10139 are not shown because of problems with one or more of the *IRAS* fluxes for these objects.

The Mira variable with the youngest shell, $1.2 \times 10^4$ years old, is Mira itself. W Peg's shell is $1.6 \times 10^5$ years old, the oldest of any of the Miras. Evidence that the nearby unresolved Miras do not have less dense shells is provided by the PSC 12 $\mu$m fluxes. The 12 $\mu$m emission should arise from the inner portion of the CSS. If the unresolved shells are less dense than those which are resolved, one would expect them to have lower 12 $\mu$m intensities. However, if we normalize the PSC fluxes by the distance squared, there is no significant difference between the 12 $\mu$m fluxes of the resolved and unresolved groups.

There are several ways by which we could estimate the lifetime of a Mira, using our age calculations. The simplest way is to take the average age of the resolved Mira shells in Table 1 and assume that on average these stars have lived half of their Mira lifetimes. This yields a lifetime of $1.1 \times 10^5$ yr. This is apt to be an overestimate, since an old star has a greater chance of being resolved than does a young star. Some of the nearby unresolved stars in Table 3 may be young Miras with small shells. Let's assume for the moment that all the nearby unresolved Miras have shells which are slightly smaller than our resolution threshold. We required the outer radius to be at least 2′ in order for the shell to be considered resolved. We can use equations (5a) and (5b) to calculate how long these stars would require to produce a shell of this size. Assuming that these stars do not have large, tenuous shells, this gives the maximum age for each of these Miras. For the 19 unresolved Miras within 500 pc, this maximum age is $3.6 \times 10^4$ yr on average. If we now assume that these unresolved stars have lived half of their maximum age and combine this result with the average ages of the resolved Miras within 500 pc, we obtain an estimated lifetime of $6.5 \times 10^4$ yr. This is apt to be an underestimate, because as discussed above, the nearby Miras may have large shells which *IRAS* could not detect. This estimate again suggests that the lifetime of a Mira is $\sim 10^5$ yr, excluding any period before the star begins to lose mass at a detectable rate. This is twice the estimated lifetime obtained by comparing the numbers of Miras and planetary nebulae in our Galaxy (Wood 1990), and the discrepancy may indicate that not all Miras produce planetary nebulae.

Because most of the carbon stars within 600 pc which were processed are resolved (24 out of 38, ignoring IRC + 10216), the ages of these stars can be used to estimate the duration of the carbon star phase for stars in the solar neighborhood. If we assume that these stars are, on average, halfway through the carbon star phase, the average age of $1.1 \times 10^5$ yr implies the duration of this phase is about $2 \times 10^5$ yr. This result agrees with the carbon star lifetime derived by Claussen et al. (1987), who estimated that the carbon star phase lasts for $10^5$–$10^6$ yr. From the distribution of carbon stars in the TMSS, these authors deduce that carbon stars had main-sequence masses between 1.2 and 1.6 $M_\odot$. They obtained their upper limit age by dividing the envelope mass that must be shed ($\sim 0.8\ M_\odot$) by the average mass-loss rate ($\geq 2 \times 10^{-7}\ M_\odot\ \mathrm{yr}^{-1}$). Their lower limit is set by the birthrate of the main-sequence F stars they believe evolve into carbon stars. On the other hand our estimate is an order of magnitude longer than the lifetime of $2 \times 10^4$ yr calculated by Willems & de Jong (1988). Even if the interaction of the CSS with the ISM is ignored, and the age is calculated by simply dividing the CSS size by the molecular expansion velocity, and all of the unresolved stars are assumed to have an age of 0 yr, the average is $6.1 \times 10^4$ yr, implying a carbon star lifetime of $1.2 \times 10^5$ yr. One potential source of error in our calculation is that the molecular velocity has been used, rather than the unknown dust expansion velocity. However, the dust velocity would have to be at least 5 times as large as the molecular velocity, requiring an average drift velocity of $\geq 80$ km s$^{-1}$ to force the lifetime calculated here to match that of Willems and de Jong. A drift velocity this large will result in grain sputtering and also implies a dust density which is too low to produce the flux detected by *IRAS* at a reasonable temperature (see § 2.4). Bringing our estimate for the carbon star lifetime into agreement with Willems & de Jong would require that all or most of the CSS material at large radii is oxygen-rich. It is not clear whether the composition of the dust at large radii can be determined spectroscopically. While a few carbon stars do show the 9.7 $\mu$m silicate feature in their *IRAS* low-resolution spectra (Willems & de Jong 1986), probably arising from material expelled when the star had an oxygen-rich envelope, the overwhelming majority do not. Willems & de Jong (1986) estimate that the silicate feature will disappear $\sim 100$ yr after the abundance of carbon exceeds that of oxygen, but van der Vee & Habing (1988) report that about 30% of stars in region V of their *IRAS* two-color diagram, which is populated by stars with detached shells, show the 9.7 $\mu$m feature in absorption. It seems unlikely that such a large fraction of these stars would exhibit this spectral feature if it disappeared only 100 yr after the cessation of mass loss.

Not surprisingly, the resolved stars have redder [100 − 60 $\mu$m] $\equiv \log_{10}$(100 $\mu$m flux/60 $\mu$m flux) colors on average than do the unresolved objects. Only one of the stars with [100 − 60 $\mu$m] $< -0.54$ was resolved, while all but one of the stars with [100 − 60 $\mu$m] $> -0.37$ (including NGC 6720 and NGC 2346 which are not shown in Fig. 5) were resolved. However, many of the extended stars have *bluer* [25 − 12 $\mu$m] colors than the nearby unresolved stars. All but one of the objects with [25 − 12 $\mu$m] $< -0.475$ were found to be extended. A [25 − 12 $\mu$m] value less than $-0.56$ corresponds to a temperature of 2000 K or more, and indicates that there is very little dust close to the star. If the resolved objects are older than the unresolved objects, their bluer [25 − 12 $\mu$m] color is additional evidence that the mass-loss process is increasingly episodic as the star ages. With the exception of the S star RZ Sgr, the objects with the reddest [100 − 60 $\mu$m] colors are all carbon stars. This 100 $\mu$m excess has been noted by several authors and has been analyzed by Egan & Leung (1991), who modeled the IR emission from carbon stars and found that a large ($\sim 1$ pc) detached outer shell is required to produce the *IRAS* 25, 60, and 100 $\mu$m fluxes.

One final difference between the nearby resolved and unresolved groups is the much higher percentage of semiregular variables in the resolved group. The percentage of Miras and semiregulars is 58% and 21%, respectively, in the unresolved group, but 25% and 63% in the nearby resolved group. Semiregulars are more common in the nearby resolved group even if the oxygen-rich or carbon stars are considered separately, or if the SRc stars (which are supergiants not on the AGB) are eliminated, or if all the unresolved stars of unknown type are counted as semiregulars. The prevalence of semiregular variables in the resolved group is surprising; these variables have a much smaller average amplitude of variation than do Miras, and at least among Mira variables the mass-loss rate is positively correlated with the amplitude of the star (Whitelock, Pottasch, & Feast 1987).

There are three simple effects that could cause the semiregular variables to have larger shells than the Miras; their

shells could be expanding more rapidly, they could have higher mass-loss rates producing denser, more easily detected shells, or they could have been losing mass for a longer time than the Miras. If the velocity from the CO observations is a good indication of the dust expansion velocity, then the resolved semiregulars are not expanding faster than the resolved Miras, because the two groups have nearly identical average CO velocities. The average mass-loss rate for resolved semiregulars is only about half the average value for the resolved Miras, so their shells should be *less* dense, on average. It is conceivable that the semiregulars have larger shells because their lower mass-loss rates allow the dust to decouple from the gas at a smaller radius, and thereby develop a larger drift velocity. However, this would imply that the size of a dust shell should be anticorrelated with the mass-loss rate (if the mass-loss rate is constant). Instead, the shell sizes and mass-loss rates in Table 1 show a weak (and probably insignificant) positive correlation. The most likely explanation seems to be that the semiregular variables have on average been losing mass longer than have the Miras.

### 2.3. *The Interaction of the Shells with the ISM*

The resolved stars are all less distant than 1 kpc, and most are within 500 pc. Being this nearby, almost all of these objects have measurable proper motions, which allows us to calculate ($\boldsymbol{v}_{\rm LSR}$). Borkowski & Sarazin (1990) have found that the envelopes of planetary nebulae with large velocities relative to the local ISM are often distorted by the ISM ram pressure. The simple model fitted by the MFP includes this effect only insofar as the model is ellipsoidal. Distortion caused by the ISM might increase the eccentricity of the fitted shell. Any distortion should be most easily seen in larger shells which, for a given $\dot{M}$ and $v_0$, will have less dense outer edges more easily deformed by the ISM ram pressure. However, no correlation was found between the eccentricity of the shell and the shell size. Because ram pressure increases quadratically with the star's velocity with respect to the ISM, and since this velocity will nearly equal $\boldsymbol{v}_{\rm LSR}$ in the solar neighborhood, the shells of stars with large $|\boldsymbol{v}_{\rm LSR}|$ should suffer the greatest distortion, but no such correlation is seen. The shells of stars near the Galactic plane are no more eccentric than those located far from the plane, where the ISM density should be less. Finally, there is no correlation between $\dot{M}$ and the eccentricity. We therefore find no evidence in this study that the shape of the CSS is distorted as a result of ram pressure from the surrounding ISM. Perhaps the eccentricity caused by bipolar outflow dominates any effect of ram pressure from the ISM.

### 2.4. *The Dust Temperature*

The estimated shell masses from Table 1 can be combined with the extended emission flux values from Table 3 of Paper I, to calculate mean temperatures for the resolved region of the dust shells. Hildebrand (1983) showed that for spherical dust grains

$$M_{\rm shell} = \frac{F(\nu)D^2}{B(\nu, T)} \frac{4/3a\rho}{Q(\nu)} \left(\frac{M_{\rm gas}}{M_{\rm dust}}\right), \qquad (6)$$

where

$M_{\rm shell}$ = the mass of the resolved portion of the dust shell,
$F(\nu)$ = the 60 $\mu$m flux from the resolved region,
$D$ = the distance to the star,
$B(\nu, T)$ = the Planck function at frequency $\nu$ and temperature $T$,
$a$ = the radius of a dust grain,
$\rho$ = the density of the dust material, assumed here to be 3 g cm$^{-3}$,
$Q(\nu)$ = the emissivity of the dust at frequency $\nu$,
$M_{\rm gas}/M_{\rm dust}$ = the gas-to-dust mass ratio, assumed here to be 100.

An iterative procedure was used to find a temperature which satisfied equation (6), for each resolved shell except that of NGC 6720, for which no mass-loss rate was available. The mass of the material within a radius of 1′ was subtracted from the mass listed in Table 1 to produce an estimate of the mass of the resolved region. The dust grains were assumed to have radii of 0.1 $\mu$m, and a 60 $\mu$m emissivity of 0.0046 was used. This emissivity was obtained by interpolating values tabulated by Draine (1987). The emissivities of graphite spheres and spheres of "astronomical silicate" differ negligibly at 60 $\mu$m. The 60 $\mu$m flux values from Table 3 of Paper I were multiplied by 1.03, to color correct them for a 40 K blackbody.

Figure 6*a* shows a histogram of the temperatures calculated by solving equation (6). The average and median temperatures are 37 and 35 K, respectively. The average outer radius for these shells is 0.57 pc. Collison & Fix (1991) modeled the temperature profiles of axisymmetric circumstellar dust shells by solving the radiative transfer problem. They found that all temperature profiles exhibited the same basic shape

$$T(r) = T_0\left(\frac{r_0}{r}\right)^{0.4} e^{-\xi(1-r_0/r)} \approx T_0\left(\frac{r_0}{r}\right)^{0.4} e^{-\xi} \quad (r \gg r_0)\,, \qquad (7)$$

where $r_0$ is the radius at which dust condenses with a temperature of $T_0$, and $\xi$ ranges from 0.48 near the pole to 0.86 near the equator of their model shells. Equation (7) implies that the temperature at large $r$ is not strongly dependent upon $r$, so the average temperature of 37 K obtained by solving equation (6) should be a good estimate of the temperature at half the average outer radius (0.29 pc). This temperature is in fair agreement with the value of 30 K obtained from equation (7) with $T_0 = 1000$ K, $r_0 = 50$ AU, $\xi = 0.67$ (these are typical values for $T_0$ and $r_0$ from the models of Collison & Fix; this value of $\xi$ is the average of the polar and equatorial values), and $r = 0.29$ pc.

Figure 7 shows the radial dependence of $I_{60\,\mu\rm m}/I_{100\,\mu\rm m}$ for the stars which were found to be extended in the 100 $\mu$m data. IRC+10216 was not included, because of the low reliability of its 60 $\mu$m model parameters. This ratio decreases for all the stars from a radius of 0.1 pc to a radius $\approx$0.5 pc. Assuming there is no radial gradient in the grain emissivity, this decrease must arise from a decrease in dust temperature. The dust within this region must be heated either by radiation from the central star, or by collisions with the expelled gas. The data become progressively more noisy as the edges of the envelopes are approached, but the four stars (V Eri, W Pic, RY Dra, and R CrB) with the largest envelopes show that $I_{60\,\mu\rm m}/I_{100\,\mu\rm m}$ stops decreasing at a radius of about 0.9 pc. The nearly constant ratio beyond 0.9 pc indicates that in the outer envelope the dust is externally heated.

These temperature gradient regimes have been noted separately in earlier work. Hawkins (1990) presented *IRAS* 60 $\mu$m and 100 $\mu$m maps of W Hya obtained from the same survey data used here, and also found it to be extended in both bands. The maps show the CSS has a radius of 15′–20′. This is in fair

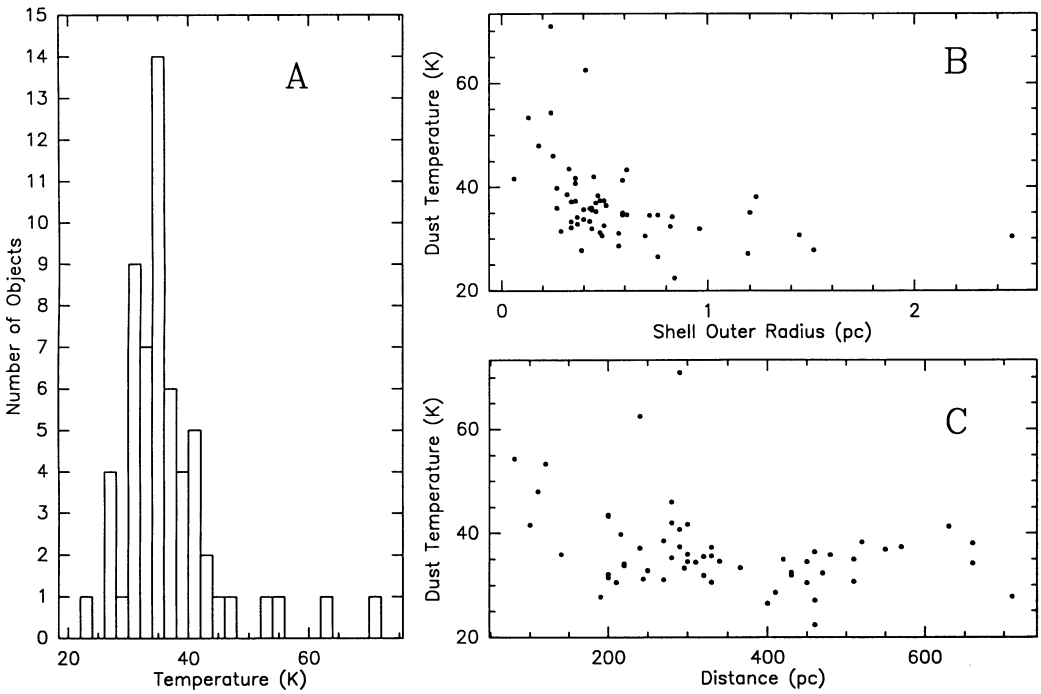


FIG. 6.—(*a*) Histogram of calculated dust temperatures. Four of the shells, those of R Leo (53 K), W Hya (54 K), R Crt (63 K), and U Hya (71 K) seem to be significantly warmer than average. (*b*) Distribution of calculated shell temperatures as a function of the shells' outer radii. Note that the warmest shells are much smaller than average, therefore the average temperature of the dust should be higher. (*c*) Calculated shell temperatures as a function of distance. All of the warmest shells are also closer than average, allowing material nearer the star to be resolved.

agreement with the 10′ 60 $\mu$m and 15′ 100 $\mu$m sizes for this object listed in Table 3 of Paper I, obtained from the MFP. Hawkins compared the 60 and 100 $\mu$m data and derived a dust temperature of $\sim$40 K in the outer envelope, in good agreement with the average temperature of 37 K obtained by solving equation (6). He found that $I_{60\,\mu m}/I_{100\,\mu m}$ decreases radially and showed that this is consistent with radiative heating of the dust by W Hya. Though not remarked upon by the author, the Hawkins data also indicate $I_{60\,\mu m}/I_{100\,\mu m}$ no longer decreases beyond a radius of 0.33 pc (assuming the distance used here, 80 pc, rather than 115 pc used by Hawkins). For R CrB, Gillet et al. (1986) found that $I_{60\,\mu m}/I_{100\,\mu m}$ is constant across the entire 18′ diameter shell, excluding an unresolved central hot spot which covers the inner 1 pc radius of the shell. The dust tem-

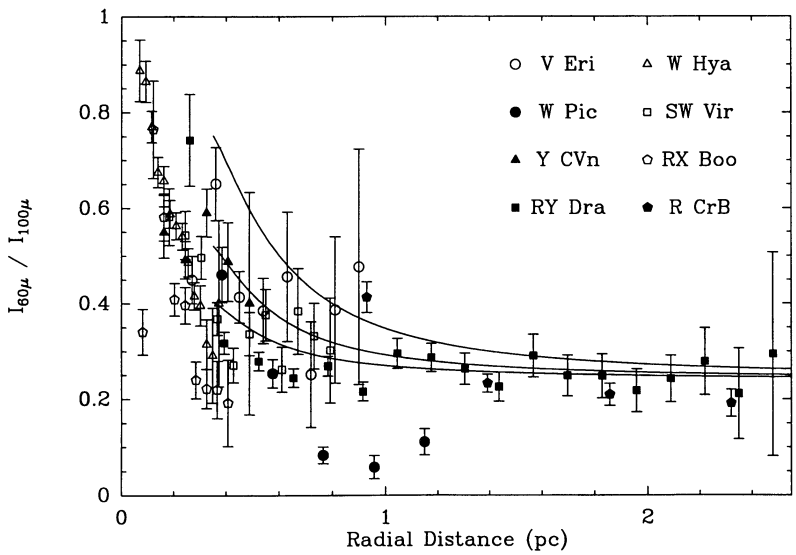


FIG. 7.—Radial dependence of the ratio of the 60 and 100 $\mu$m brightness is shown for the stars which are extended in the 100 $\mu$m data. In this figure, the raw CRDD data have been summed after baseline removal in 1′ wide annular bins of increasing radial distance from the central star. Filled symbols, for W Pic, Y CVn, RY Dra, and R CrB, represent carbon star data. Data at radii smaller than 2′ are not shown. Several points from radii less than 0.2 pc with $I_{60\,\mu m}/I_{100\,\mu m} > 1.0$ are not shown. The error bars represent the value of $\sigma(60\ \mu m/100\ \mu m) \equiv (1/I_{100\,\mu m})[(\sigma^2_{60\,\mu m}/N_{60\,\mu m}) + (I^2_{60\,\mu m}\sigma^2_{100\,\mu m}/I^2_{100\,\mu m}N_{100\,\mu m})]^{1/2}$ where $\sigma_{60\,\mu m}$ and $\sigma_{100\,\mu m}$ are the standard deviations in $I_{60\,\mu m}$ and $I_{100\,\mu m}$, and $N_{60\,\mu m}$ and $N_{100\,\mu m}$ are the numbers of points in the annular bins. For clarity of the figure, the very substantial error bars for the abscissa are not shown. The curves are from the model of Gillet et al. (see text).

perature inferred by the authors is 25–30 K. Both of these earlier works, plus the results in Figure 7, indicate that within the central $\sim 0.5$ pc the dust is heated primarily by the central stars' radiation, while an external heat source dominates beyond about 1 pc.

Gillet et al. (1986) developed a model for the radial temperature profile and infrared brightness of an envelope heated by both its central star and an external heat source, the effects of which are constant throughout the envelope. This model was used to produce the three curves shown in Figure 7. The three curves represent the expected value of $I_{60\,\mu m}/I_{100\,\mu m}$ for stars of $10^4\ L_\odot$ (upper curve), $5 \times 10^3\ L_\odot$, and $3 \times 10^3\ L_\odot$ (lowest curve). In all three cases the central star was assumed to be at a distance of 340 pc and emit as a 2500 K blackbody, the dust emissivity $\propto \lambda^{-1}$, and the external heating rate is equivalent to that of a $10^4\ L_\odot$ star at a radius of 0.9 pc. The curves are truncated at 0.4 pc (4′), because at smaller radii the value of $I_{60\,\mu m}/I_{100\,\mu m}$ becomes very sensitive to the orientation of the *IRAS* detector with respect to the central star. Lowering the exponent of the dust emissivity ($m$) below $-1$ causes $I_{60\,\mu m}/I_{100\,\mu m}$ to increase, for a fixed rate of external heating. By calculating models with no external heating we can place a lower limit on the value of $m$ by requiring $I_{60\,\mu m}/I_{100\,\mu m}$ to match the data at large radii. For a $10^4\ L_\odot$ model, $m$ cannot go below $-1.4$, and for a $3 \times 10^3\ L_\odot$ model $m$ must be greater than $-1.6$, to match the color near 1 pc. It should be emphasized that changing $m$ cannot remove the need for an external heat source, because central heating cannot produce the flat color distribution seen beyond 1 pc.

In § 3.5 it was shown that our results indicate that the carbon star phase of evolution lasts substantially longer than the lifetime estimate of Willems & de Jong (1988). One way in which our results could be brought into agreement with those of Willems and de Jong is by assuming that the dust has a substantially larger terminal velocity than the molecular material. This is by no means excluded by the results of some of the models of dust acceleration which can be found in the literature. For example Wickramasinghe (1972) calculated that the dust should typically be accelerated to a terminal velocity of several thousand km $s^{-1}$! However if the dust is expanding at a much higher velocity than the molecular material, then equation (3) tells us that the density of the dust in the CSS must be less than the value that the molecular expansion velocity and the dust/gas ratio near the star would suggest. This means that we must obtain the far-infrared fluxes measured by *IRAS* from a much smaller total amount of solid material. If we assume the dust velocity is 5 times that of the CO (the minimum increase required to make our carbon star age estimates consistent with Willems & de Jong's lifetime estimate), then equation (6) must be solved with a correspondingly smaller effective dust/gas ratio. This increases the average estimated dust temperature from 37 to 50 K, which does not agree as well with the 30 K predicted by equation (7), or the temperatures implied by $I_{60\,\mu m}/I_{100\,\mu m}$.

## 3. NOTES ON PARTICULAR OBJECTS

*W Pictoris*: The 18.′4 radius of the 100 $\mu$m emission surrounding this star (see Fig. 18*d* of Paper I) is the second largest of any of the CSSs presented here (after R CrB), corresponding to 3.5 pc (assuming a distance of 660 pc). The 60 $\mu$m emission (Fig. 6*b* in Paper I) covers a much smaller area, however no well-defined outer edge is seen in the 60 $\mu$m emission, suggesting noise may be obscuring emission from beyond a radius of $\sim 7'$. The size of the 100 $\mu$m envelope is so large, that it is questionable whether the extended emission is actually associated with the star. The extended emission at both 60 and 100 $\mu$m is well centered on the star's position, and the MFP reported the emission arises from a nearly circular region with an aspect ratio of 0.96 in both bands. The object is at a fairly high Galactic latitude ($b = -31$), however, its PSC CIRR2 flag is 4, indicating the field may be contaminated by infrared cirrus. The CIRR1 flag, which is a count of the objects within 30′ which were detected by *IRAS* only in the 100 $\mu$m band and are apt to be cirrus structures, is 0. A search of the SIMBAD and NED data bases revealed no objects within 20′ of W Pic which could produce the 100 $\mu$m emission.

Assuming the 100 $\mu$m emission is circumstellar in origin, the mass-loss rate and outflow velocities derived from CO observations (Olofsson, Eriksson, & Gustafsson 1988) imply that near the outer edge the CSS has a density of only $4 \times 10^{-3}$ H $cm^{-3}$. Even at this star's distance of 330 pc above the Galactic plane, the surrounding ISM should be dense enough that the CSS would require more than $10^6$ yr to expand to 3.5 pc. It therefore seems likely that in order for the CSS to reach this size, either W Pic must lie in a region of very low ISM density, or its mass-loss rate must have been much greater in the past, or our distance estimate must be much too high.

*RY Draconis*: This object is surrounded by the third most extensive region of emission of all those examined. If the extended emission is circumstellar, the radius is 2.9 pc (assuming a distance of 450 pc and using the 100 $\mu$m size). As with W Pic, the size is so large, that it is possible that the extended emission arises from a chance alignment with an object not associated with the star. RY Dra has a high Galactic latitude ($b = 51°$), so it is unlikely that this region is contaminated by infrared cirrus. Also, the PSC CIRR1 and CIRR2 flags are 0 and 3, respectively, indicating the region is relatively free of cirrus contamination. We obtained $2° \times 2°$ FRESCO (IPAC 1989) images centered on RY Dra. They reveal very little cirrus contamination at 60 $\mu$m. There is cirrus emission visible in the 100 $\mu$m image, but it is neither as intense nor as large as the extended emission surrounding RY Dra. A search of the SIMBAD and NED data bases revealed only two cataloged objects within 20′ of RY Dra; SAO 15949, a 10th magnitude F2 star 9′ away and IRAS F12532+6600, a faint galaxy 17′ away whose 60 $\mu$m flux is 2.5 mJy, and which was undetected at 100 $\mu$m. Neither of these objects could be responsible for the extended emission around RY Dra.

RY Dra differs from W Pic in that the size and shapes of the 60 and 100 $\mu$m regions are very similar (see Figs. 10*b* and 19*c* in Paper I). Throughout most of the extended emission, $I_{60\,\mu m}/I_{100\,\mu m} \approx 0.25$ which is near the middle of the range for infrared cirrus clouds (Low et al. 1984). If the extended emission is circumstellar in origin, the temperature of the dust shell is nearly constant throughout the outer envelope. As with W Pic, the CO-derived mass-loss rate and outflow velocity (Olofsson, Eriksson, & Gustafsson 1987) imply a very low density near the outer edge of the CSS, again indicating that either the surrounding ISM has a very low density, or the star's mass-loss rate was greater in the past.

*NGC 6720 (the Ring Nebula)*: Hawkins & Zuckerman (1991, hereafter HZ) also analyzed the survey data for this object, by performing a one-dimensional deconvolution. The results they obtained differ significantly from those presented here. The 60 $\mu$m diameter they obtained is 50″, far smaller than the 10′ diameter we obtained. The source of this disagreement is

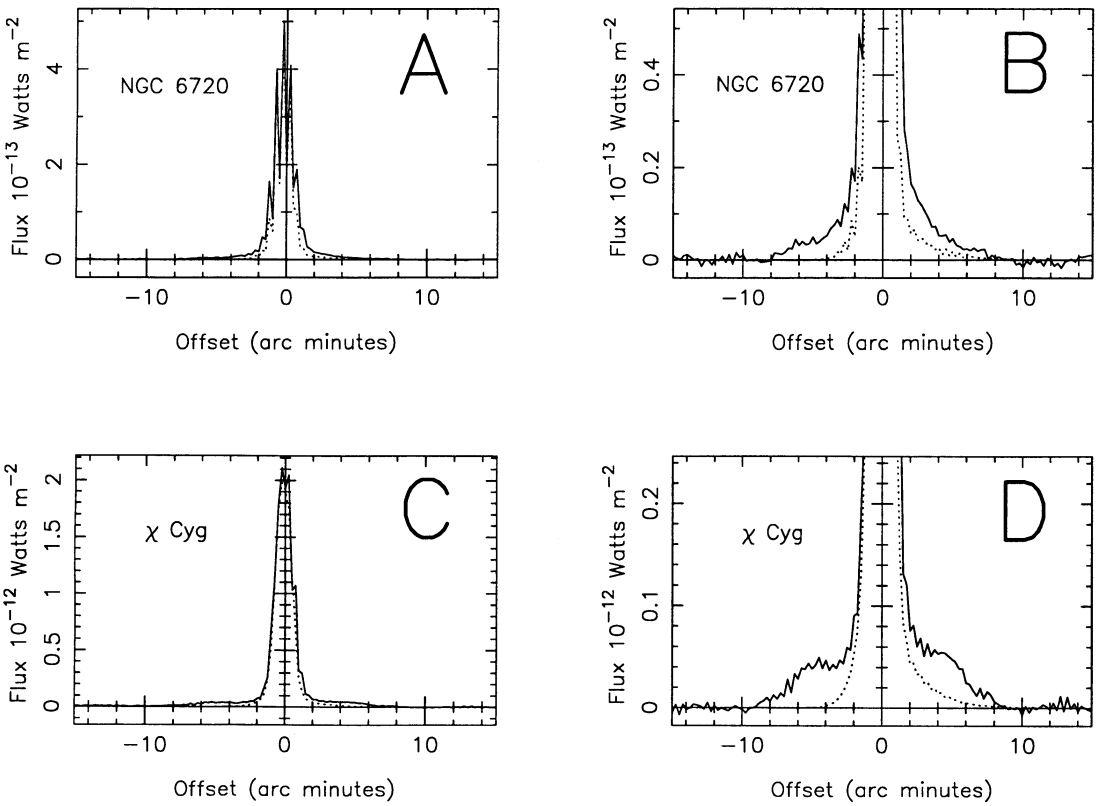


FIG. 8.—(*a*) The 60 μm data for NGC 6720, binned as in Fig. 1. The dotted line shows the best-fit point source for these data. (*b*) Same data shown in (*a*), but with an expanded vertical scale. Note that emission is seen several arcminutes further from the source than can be explained by the detector's point-spread function alone. (*c*) Binned data for χ Cygni (*solid line*) and the best-fit point source (*dotted line*). The extended emission region is very flat, suggesting the CSS is hollow. (*d*) Same data as in panel (*c*) plotted with an expanded vertical scale.

shown in Figures 8*a* and 8*b*. The HZ diameter is a full width at half-maximum, whereas the MFP reports a size at zero intensity. Since the extended emission is very weak, it has very little effect on the FWHM. However, HZ also examined the individual detector scans in an attempt to find low-level emission which might arise from a weak infrared halo, and found none. We believe that because our program fit a model to all the scans passing near the object, it lowered the noise floor by averaging, and this allowed us to detect extended emission that is too faint to be seen in individual scans.

*χ Cygni*: This object is not listed in Table 1 or Table 3 of Paper I, because its PSC CIRR2 flag is 5, which indicates the field may be contaminated by infrared cirrus. Nevertheless, this object does appear to be extended (see Figs. 8*c* and 8*d*), and the 60 μm survey scans covering the object have reasonably flat baselines. Unfortunately the 100 μm scans show abundant evidence of cirrus contamination. The 60 μm shell has a radius of 7′, and it is strikingly flat-topped, implying that the shell is detached, with an inner radius of 3′.5. If a distance of 115 pc (Stein 1991) is adopted, the inner and outer radii are 0.12 and 0.23 pc, respectively, and the shell age obtained by solving equations (5a) and (5b) is $3.5 \times 10^4$ yr. Further evidence that χ Cygni has a detached shell is provided by its *IRAS* [12−25] and [25−60] colors, which correspond to a temperature of 2000–2500 K. This indicates most of the infrared radiation from this star arises from the star's photosphere. This is in sharp contrast to the situation for most of the AGB stars with detectable molecular emission, the colors of which usually indicate the presence of dust at a temperature below 1000 K. Had this star not been rejected due to its CIRR2 flag (which is only 1 unit above the rejection threshold), it would have been the best example of a detached shell in the entire sample. However, χ Cygni is located only 7 pc above the Galactic plane, so the detached shell might be composed of swept-up ISM material, and may not indicate that the star's mass-loss rate was greater in some past era. The *IRAS* small-scale structure catalog does not list χ Cygni.

## 4. CONCLUSIONS

The *IRAS* survey data for 512 red giant stars were processed using a simple model fitting program. This program was developed to detect the presence of low-intensity extended emission surrounding a bright unresolved source. Of these stars, 76 were found to have shells which are resolved in the *IRAS* 60 μm data. The average shell radius is 0.74 pc. Forty percent of the 76 resolved stars have carbon-rich envelopes. A model for the interaction of the expanding shell with the surrounding ISM was developed. This model predicts that the edges of the largest shells (those with radii >1 pc) will be expanding at much lower speeds than the inner envelope, where the CO emission arises. From examining the resolved envelopes we conclude the following:

1. Most of the CSSs, including many surrounding stars which have been losing mass for $\sim 10^5$ yr, have small total masses. Yet NGC 2346 and IRC+10216 are surrounded by much more massive envelopes, implying that duration of the "superwind" is only a small fraction of star's AGB lifetime.
2. The average age for the shells surrounding the 13 Mira-

type stars which are extended is $6 \times 10^4$ yr. This suggests that the period during which these stars lose mass lasts for $\sim 10^5$ yr. The oldest shell found surrounds W Peg, and the youngest surrounds Mira itself.

3. Some shells appear to be detached from the central star and have resolved inner radii.

4. Most of the shells with inner radii of 0.25 pc or less have detectable CO emission, while most with inner radii larger than 0.3 pc (such as R CrB) do not. The simplest explanation for this is that CO is destroyed by the interstellar UV field at a radius of about 0.3 pc.

5. Although all but one of the eight stars less distant than 200 pc are resolved in the *IRAS* 60 $\mu$m data, 33 stars within 500 pc with CO envelopes, were not. These stars probably have younger CSSs than those which were resolved.

6. Almost all the carbon stars with distances of 500 pc or less have resolved shells, while only half of the oxygen-rich stars do. The resolved carbon star shells also are older on average than the oxygen-rich ones. These facts imply that carbon stars have been losing mass for a longer period, on average, than oxygen-rich red giants. The average age of these nearby carbon stars is $1.1 \times 10^5$ yr, which indicates the lifetime of an average carbon star is $\sim 2 \times 10^5$ yr.

7. Most of the nearby unresolved stars from the CO selected list are Mira variables, while most of the nearby resolved stars are semiregular variables. The simplest explanation for this is that the semiregular variables have been losing mass for a longer period than the Miras.

8. Radiative transfer models and the value of $I_{60\,\mu m}/I_{100\,\mu m}$ allow the average dust temperature in the outer regions of a CSS to be estimated. The typical value obtained is about 35 K. This provides a constraint on the value of the dust drift velocity, because a very large drift velocity results in a low dust density in the outer shell which in turn requires a high dust temperature to produce the 60 and 100 $\mu$m fluxes measured by *IRAS*. The radial dependence of $I_{60\,\mu m}/I_{100\,\mu m}$ suggests that an external heat source supplies most of the thermal energy to the dust beyond a radius of 1 pc.

We would like to thank the staff of IPAC for their help in processing the raw data. Also, we thank Nicolas Mauron, Robert Stencel and Wendy Bauer, who contributed many helpful comments after reading an early draft of this paper. Finally the contribution of an anonymous referee, whose comments resulted in many improvements and the removal of a great deal of chaff, is gratefully acknowledged. This work was supported by NASA contract NAG 5-1153 and NSF contract AST 90-15755.

## REFERENCES

Aumann, H. H., Fowler, J. W., & Melnyk, M. 1990, AJ, 99, 1674
Berruyer, N., & Frisch, H. 1983, A&A, 126, 269
Borkowski, K. J., & Sarazin, C. L. 1990, ApJ, 360, 173
Bowers, P. F., & Hagen, W. 1984, ApJ, 285, 637
Celis, L. S. 1981, A&A, 99, 58
Cesaroni, R., Palagi, F., Felli, M., Catarzi, M., Comoretto, G., Di Francos, Giovanardi, C., & Palla, F. 1988, A&AS, 76, 445
Claussen, M. J., Kleinmann, S. G., Joyce, R. R., & Jura, M. 1987, ApJS, 65, 385
Collison, A. J., & Fix, J. D. 1991, ApJ, 368, 545
Deguchi, S., Nakada, Y., & Sahai, R. 1990, A&A, 230, 339
Dougados, C., Rouan, D., & Léna, P. 1992, A&A, 253, 464
Draine, B. T. 1987, unpublished supplement to Draine & Lee (1984)
Draine, B. T., & Lee, H. M. 1984, ApJ, 285, 89
Eaton, J. A., & Johnson, H. R. 1988, ApJ, 325, 355
Egan, M. P., & Leung, C. M. 1991, ApJ, 383, 314
Engels, D., & Heske, A. 1989, A&AS, 81, 323
Fouqué, P., Le Bertre, T., Epchtein, N., Guglielmo, F., & Kerschbaum, F. 1992, A&AS, 93, 151
Gail, H. P., & Sedlmayr, E. 1985, A&A, 148, 183
Gatewood, G. 1992, PASP, 104, 23
Gillet, F. C., Backman, D. E., Beichman, C., & Neugebauer, G. 1986, ApJ, 310, 842
Goldreich, P., & Scoville, N. 1976, ApJ, 205, 144
Hawkins, G. W. 1990, A&A, 229, L5
Hawkins, G. W., & Zuckerman, B. 1991, ApJ, 374, 227
Hekkert, P. L., Versteege-Hensel, H. A., Habing, H. J., & Wiertz, M. 1989, A&AS, 78, 399
Herman, J., & Habing, H. J. 1985, Phys. Rept., 124, 4
Heske, A. 1989, A&A, 208, 77
Hildebrand, H. 1983, QJRAS, 24, 267
Huggins, P. J., & Healy, A. P. 1986, MNRAS, 220, 33P
Iben, I., & Renzini, A. 1983, ARA&A, 21, 271
IPAC, User's Guide, 1989 (JPL D-2416)
*IRAS* Point Source Catalog, 1985, Joint *IRAS* Working Group (Washington: GPO)
Judge, P. G., & Stencel, R. E. 1991, ApJ, 371, 357
Jura, M., & Kleinmann, S. G. 1992, ApJS, 79, 105
Kleinmann, S. G. 1989, IAU Colloq. 106, Evolution of Peculiar Red Giant Stars (Cambridge: Cambridge Univ. Press)
Knapp, G. R. 1986, ApJ, 311, 731
Knapp, G. R., & Bowers, P. F. 1988, ApJ, 332, 299
Knapp, G. R., & Morris, M. 1985, ApJ, 292, 640
Knapp, G. R., Phillips, T. G., Leighton, R. B., Lo, K. Y., Wannier, P. G., & Wootten, H. A. 1982, ApJ, 252, 616
Knapp, G. R., Sutin, B. M., Phillips, T. G., Ellison, B. N., Keene, J. B., Leighton, R. B., Masson, C. R., Steiger, W., Veidt, B., & Young, K. 1989, ApJ, 336, 822
Kwok, S. 1975, ApJ, 198, 583
Leene, A., & Pottasch, S. R. 1988, A&A, 202, 203
Letzelter, E., Eidelsberg, M., Rostas, F., Breton, J., & Thiebelmont, B. 1987, Chem. Phys., 114, 273
Low, F. J., et al. 1984, ApJ, 278, L19
Mamon, G. A., Glassgold, A. E., & Huggins, P. J. 1988, ApJ, 328, 797
Margulis, M., Van Blerkom, D. J., Snell, R. L., & Kleinmann, S. G. 1990, ApJ, 361, 673
Mihalas, D., & Binney, J. 1981, Galactic Astronomy (New York: W. H. Freeman)
Morris, M. 1980, ApJ, 236, 823
Nyman, L. A., et al. 1992, A&AS, 93, 121
Olofsson, H. 1988, Space Sci. Rev. 47, 145
———. 1989, IAU Colloq. 106, Evolution of Peculiar Red Giant Stars (Cambridge: Cambridge Univ. Press)
Olofsson, H., Eriksson, K., & Gustafsson, B. 1987, A&A, 183, L13
———. 1988, A&A, 196, L1
Onako, T., de Jong, T., & Willems, F. J. 1989, A&A, 218, 169
Reid, N., Tinney, C., & Mould, J. 1990, ApJ, 348, 98
Rowan-Robinson, M., Lock, T. D., Walker, D. W., & Harris, S. 1986, MNRAS, 222, 273
Sivagnanam, P., Le Squeren, A. M., & Foy, F. 1988, A&A, 206, 285
Spitzer, L. 1978, Physical Processes in the Interstellar Medium (New York: Wiley)
Stein, J. W. 1991, ApJ, 377, 669
van den Bergh, S. 1984, Ap&SS, 102, 295
van der Veen, W. E. C. J., & Habing, H. J. 1988, A&A, 194, 125
van der Veen, W. E. C. J., & Rugers, M. 1989, A&A, 226, 183
Wannier, P. G., & Sahai, R. 1986, ApJ, 311, 335
Wannier, P. G., Sahai, R., Andersson, B.-G., & Johnson, H. R. 1990, ApJ, 358, 251
Whitelock, P. A., Pottasch, S. R., & Feast, M. W. 1987, Late Stages of Stellar Evolution (Dordrecht: Reidel)
Wickramasinghe, N. C. 1972, MNRAS, 159, 269
Willems, F. J., & de Jong, T. 1986, ApJ, 309, L39
———. 1988, A&A, 196, 173
Wood, P. R. 1990, From Miras to Planetary Nebulae: Which Path for Stellar Evolution? (Paris: Éditions Frontières)
Young, H. D. 1962, Statistical Treatment of Experimental Data (New York: McGraw-Hill)
Young, K., et al. 1992, in preparation
Young, K., Phillips, T. G., & Knapp, G. R. 1992b, ApJS, submitted (Paper I)
Zuckerman, B., & Dyck, H. M. 1986a, ApJ, 304, 394
———. 1986b, ApJ, 311, 345
———. 1989, A&A, 209, 119
Zuckerman, B., Dyck, H. M., & Claussen, M. J. 1986, ApJ, 304, 401